

# Implications of Bulk Velocity Structures in AGN Jets

Jianping YANG \*

*National Astronomical Observatories, Yunnan Observatory, Chinese Academy of Sciences, Kunming 650011, China; Graduate School of the Chinese Academy of Sciences, China; Yunnan Agricultural University, Kunming 650201, China*  
yangjp@mail.ynao.ac.cn

Jiancheng WANG

*National Astronomical Observatories, Yunnan Observatory, Chinese Academy of Sciences, Kunming 650011, China*

Benzhong DAI

*Department of Physics, Yunnan University, Kunming 650091, China*

Xiaoyan GAO

*National Astronomical Observatories, Yunnan Observatory, Chinese Academy of Sciences, Kunming 650011, China*

(Received 2009 April 12; accepted 2009 June 30)

## Abstract

The synchrotron self-Compton (SSC) models and External Compton (EC) models of AGN jets with continually longitudinal and transverse bulk velocity structures are constructed. The observed spectra show complex and interesting patterns in different velocity structures and viewing angles. These models are used to calculate the synchrotron and inverse Compton spectra of two typical BL Lac objects (BLO) (Mrk 421 and 0716+714) and one Flat Spectrum Radio Quasars (FSRQs) (3c 279), and to discuss the implications of jet bulk velocity structures in unification of the BLO and FR I radio galaxies (FRI). By calculating the synchrotron spectra and SSC spectra of BL Lac object jets with continually bulk velocity structures, we find that the spectra are much different from ones in jets with uniform velocity structure under the increase of viewing angles. The unification of BLO and FRI is less constrained by viewing angles and would be imprinted by velocity structures intrinsic to the jet themselves. By considering the jets with bulk velocity structures constrained by apparent speed, we discuss the velocity structures imprinted on the observed spectra for different viewing angles. We find that the spectra are greatly impacted by longitudinal velocity structures, because the volume elements are compressed or expanded. Finally, we present the EC spectra of FSRQs and FR II radio galaxies (FRII) and find that they are weakly affected by velocity structures compared to synchrotron and SSC spectra.

**Key words:** galaxies: jets – radiation mechanisms: nonthermal

## 1. Introduction

It is well known that the AGN jets radiate the strong nonthermal emission from the radio to the gamma ray range. Their spectral energy distribution (SED) consists of two bumps, attributed to the synchrotron and the inverse Compton (IC) emission of ultrarelativistic particles. The simple one-zone homogeneous jet model usually provides a good framework to explain the emissive spectra of AGN jets. However, the realistic case is that the jet has the bulk velocity structures in longitudinal and transverse directions to its axis (Blandford & Levinson 1995). To explain the spectral properties of some AGNs several authors have proposed many inhomogeneous jet models (Marscher 1980; Ghisellini et al. 1985; Georganopoulos & Marscher 1998; Wang et al. 2004; Georganopoulos et al. 2005; Tavecchio & Ghisellini 2008). For example, to reproduce the spectra of TeV blazars, Georganopoulos & Kazanas (2003a) have presented a jet model characterized by the deceleration of

bulk velocity along the jet axis. Their model is also used to explain the X-ray phenomena in kiloparsec jets of powerful radio galaxies and quasars (Georganopoulos & Kazanas 2003b). Giroletti et al. (2004a) have proposed a transverse velocity structure model, described by a slower external flow surrounding a faster spine, to explain a limb brightening morphology in Mrk 501 observed by VLBI. Ghisellini & Tavecchio (2008) have used a needle/jet model, which harbors small active regions (needles) inside a large jet, to account for the 2-3 minutes fast variability of PKS 2155-304. Recent observation of TeV blazars raise new questions regarding the one-zone uniform jet model. Such as, the unreal high Lorentz factor (about 50) demanded by avoiding  $\gamma$ - $\gamma$  absorption for TeV blazars (Krawczynski et al. 2002; Konopelko et al. 2003; Henri & Sauge 2006; Begelman et al. 2008; Finke et al. 2008) can not match the much slower speeds required by Very Long Baseline Interferometry (VLBI) observations (Piner & Edwards 2004; Piner et al. 2008). Therefore, it is argued that the jet should have velocity structures to mediate the inconsistency of bulk motions obtained by different wavebands (Chiaberge et al. 2000; Trussoni et al. 2003).

\* National Astronomical Observatories, Yunnan Observatory, Chinese Academy of Sciences, Kunming 650011, China

For unification of BL Lac objects and FR I radio galaxies, the velocity structures have also been suggested by Chiaberge et al. (2000). By analyzing the core emissions of FR I radio galaxies observed by Hubble Space Telescope, they have found that the observed fluxes of FR I nucleus are over-luminous by a factor of  $10 - 10^4$  than ones predicted by simple one-zone model, in radio and optical bands. Therefore they proposed a jet velocity structure, which a fast spine is surrounded by a slow layer, to reconcile the unification scheme.

In this paper we present the SSC and EC models of AGN jets with continually longitudinal and transverse bulk velocity structures. Our study is not completely new, but we include new ingredients and results. Firstly, the observed apparent speed is obtained by flux convolution over the whole emitting region with bulk velocity structures. Secondly, each part of the jet contributes its spectrum to the observed SED, some important characteristics are ignored in simple models with two-zone velocity structures compared to the model with continual velocity structures. Thirdly, some parameters of jet velocity structures can be constrained by the jet power or apparent speed, our models are more realistic to discuss the emissive properties of the jet with velocity structures than previous models. Fourthly, the jet velocity structures can reasonably solve the problem of the unification of BL Lacs and FR I faced by all one-zone models. Fifthly, we find that the effects of velocity structures upon the observed synchrotron and SSC spectra strongly depend on the viewing angles. Sixthly, we find that the longitudinal velocity structures, as the volume elements are compressed or expanded, have great influences upon the observed spectra. Finally, the observed EC spectra are weakly affected by velocity structures compared to the observed synchrotron or SSC ones.

In Section 2 we present the velocity structures of the jet for the models calculation and we place these modifications in the context of emission mechanisms in Section 3. We show the model application to two BL Lac objects (Mrk 421 and 0716+714) controlled by the same jet power in Section 4, focusing on the unification of BLO with FRI sources. We then discuss the apparent speeds that govern the velocity structures of the jet to constrain the observed spectra in Section 5. In Section 6, we employ the SSC and EC models to one quasar (3c 279), and discuss the effects of the velocity structures upon the EC spectra. We finish with discussions and conclusions in Section 7.

## 2. Velocity Structures

We only select a part of the stationary jet to study. For simplicity, we adopt the following assumptions: 1. The length of the studied region is a small scale (i.e., about  $1 \times 10^{17}$  cm) compared with the whole jet. Although the whole jet may be conical or other morphologies, a cylinder jet is a good approximation within a short length scale. 2. In the studied region, the jet is assumed to have the bulk velocity structures in the longitudinal or transverse directions to the jet axis. The velocity structures are

not resolved by the VLBI observation. 3. We assume that the jet is stationary and the relativistic electrons are injected continuously with a power-law energy spectra  $N(\gamma, z_0) = N_0 \gamma^{-s} \exp(-\frac{\gamma}{\gamma_{max}})$  (Finke et al. 2008). Here we mainly pay attention to the influence of the velocity structures on radiative spectra, we ignore the radiative energy loss of the electrons in the studied jet scale. However, for the jet with the longitudinal velocity structures, as its volume elements are compressed or expanded, the electron energy distribution and magnetic field in the jet will be changed follow as Georganopoulos & Kazanas (2004):  $\gamma(z) = \gamma_0(z/z_0)^{-\xi/3}$ ,  $N(\gamma, z) = N(\gamma, z_0)(z/z_0)^{-\xi(s+2)/3}$  and  $B(z) = B_0(z/z_0)^{-\xi}$ , where the  $\xi$  is the index of longitudinal velocity structures (see the next part), the subscript "0" denote the values at the studied jet base. 4. For transverse velocity structures, the magnetic fields are assumed to be a isotropic distribution in the comoving frame.

### 2.1. Longitudinal Velocity Structures

For a jet with longitudinal velocity structures, we take the Lorentz factor along the jet to be  $\Gamma(z) = \Gamma_0(\frac{z}{z_0})^\xi$ , where  $\Gamma_0$  is the Lorentz factor at the base, the  $\xi$  is the index of longitudinal velocity structures. This power-law form was earlier given by Marscher (1980), subsequently adopted by Ghisellini et al. (1985); Georganopoulos & Marscher (1998) and Li & Wang (2004).  $\xi = 0$ ,  $\xi > 0$ , and  $\xi < 0$  correspond to transition, acceleration, and deceleration phases respectively.

VLBI measurements of apparent motion for the parsec-scale radio knots have often been employed to constrain a combination of Lorentz factor and viewing angles (Vermeulen & Cohen 1994). Although VLBI monitoring of the radio knots in blazar jets has revealed several sources containing knots with apparent speeds extending out to  $30c$  (Piner et al. 2007), the typical values for TeV blazars are found to be much more modest, under  $5c$  (e.g. Giroletti et al. (2004b); Piner & Edwards (2004)). Gopal-Krishna et al. (2004) have showed that the slow apparent speeds of the knots of blazars observed by VLBI can be reconciled with the extremely relativistic bulk motion inferred from TeV flux variations (Krawczynski et al. 2002), if one considers a modest full opening angle for the parsec-scale jets. They also have showed that the actual viewing angles,  $\theta$ , of such conical jets from the line-of-sight can be substantially larger than those commonly inferred by VLBI proper motion data (Gopal-Krishna et al. 2006). Recently, they have evaluated the role of the jet opening angle on certain key parameters (i.e. the viewing angle, the apparent speed and Doppler factor) that are inferred from VLBI radio observations of blazar nuclear jets (Gopal-Krishna et al. 2007). In these papers, they have argued that the Doppler boosting of an ultrarelativistic jet, as well as the apparent proper motions, can greatly vary across the jets cross-section, and then it is important to carry out an integration of various quantities across the jet cross-section. Therefore, they have performed an integration of the (boosted) flux-weighted apparent velocity over the jet cross section to obtain the weighted observed value of the apparent velocity of the jet, when the width

of a knot cannot be resolved by VLBI observations.

For longitudinal velocity structures the observed apparent speed ( $\beta_{app} = \frac{\beta \sin \theta}{1 - \beta \cos \theta}$ ) is decided by (Gopal-Krishna et al. 2004; Gopal-Krishna et al. 2006; Gopal-Krishna et al. 2007)

$$\beta_{app,obs} = \frac{\int \beta(z) \delta^2(z) dF'_{sync}(z)}{F_{sync}}, \quad (1)$$

where the  $F_{sync}$  is the observed flux, and the  $dF'_{sync}(z)$  is the comoving flux in  $z$ . In this equation, we take the radio spectral index to be 0.

Through the radio observation, Giroletti et al. (2004b) have found that the mean value of  $\Gamma$  is 3 in the TeV sources. Piner & Edwards (2004) have presented that the jets of TeV blazars have only mildly relativistic motion which is less than  $5c$  on parsec-scales. Piner et al. (2007) have found that the apparent speed distribution shows a peak at low speed for BL Lac objects. We then take the speed of  $\beta_{app,obs} = 3.6c$  to limit  $\Gamma_0$ .

## 2.2. Transverse Velocity Structures

For a jet with transverse velocity structures, we suppose the jet bulk velocity to be  $\Gamma(R) = \Gamma_c - (\Gamma_c - \Gamma_m)(R/R_0)^\zeta$ , where  $\Gamma_c$  and  $\Gamma_m$  are the Lorentz factor of the central and marginal region respectively. In this work, we only adopt  $\zeta$  to be 0 and 1, corresponding to different transverse velocity structures.

We take the apparent speed given by  $\beta_{app,obs} = 3.6c$  to restrict  $\Gamma_c$  and  $\Gamma_m$ . We also use the jet power given by (Celotti et al. 1997; Ghisellini et al. 2005)  $P_{jet} = \int_0^{R_0} \Gamma^2(R) U \beta(R) c 2\pi R dR$  to limit  $\Gamma_c$  and  $\Gamma_m$ , where  $U = U_B + U_e + U_p$  is the total energy density in the jet frame.

## 3. Radiation Mechanisms

In this section, the radiation models of continually longitudinal and transverse velocity structures are constructed respectively.

### 3.1. Radiation Model of Longitudinal Velocity Structures

We present a modified homogeneous SSC model to reproduce the entire spectral energy distribution. In the following, a prime accent denotes a parameter expressed in the comoving frame.

For an isotropic electron distribution, the synchrotron emission coefficient is given by

$$j'_s(\nu'_s, z) = \frac{1}{4\pi} \int N_e(\gamma, z) P_e(\nu'_s, \gamma) d\gamma, \quad (2)$$

where  $\nu'_s$  is the frequency in the comoving frame, and  $P_e(\nu'_s, \gamma)$  is the mean emission coefficient for a single electron averaged over an isotropic distribution of pitch angles. The differential synchrotron luminosity between  $z$  and  $z + dz$  is then given by

$$dL'_s(\nu'_s, z, \theta) = 4\pi^2 R_0^2 j'_s(\nu'_s, z) e^{-\frac{\alpha'_s(\nu'_s, z) R_0}{\sin \theta}} dz, \quad (3)$$

where  $R_0$  is the radius of jet,  $\alpha'_s(\nu'_s)$  is the absorption coefficient (Rybicki & Lightman 1979) as follows

$$\alpha'_s(\nu'_s, z) = -\frac{1}{8\pi m_e \nu'^2_s} \int \gamma^2 \frac{d}{d\gamma} \left[ \frac{N_e(\gamma, z)}{\gamma^2} \right] P_e(\nu'_s, \gamma) d\gamma. \quad (4)$$

The Doppler factor is given by  $\delta(z, \theta) = \frac{1}{\Gamma(z)[1 - \beta(z)\cos\theta]}$  and  $\Gamma(z) = \Gamma_0(\frac{z}{z_0})^\xi$ , where  $\Gamma(z) = [1 - \beta^2(z)]^{-1/2}$  is the bulk Lorentz factor and  $\beta(z)$  is the velocity in the unit of  $c$ . Then the synchrotron flux density in the observe frame is simply given by

$$dF_{sync}(\nu_s, z, \theta) = \frac{1}{4\pi d_l^2} \delta^{(2+\alpha)}(z, \theta) [1 + z_{rs}] dL'_s(\nu'_s, z, \theta), \quad (5)$$

where  $\alpha$  is the spectral index and is taken as 1.0.  $d_l$  is the luminosity distance and  $z_{rs}$  is the redshift. We transfer  $\nu'_s$  into the observer's frame following as:

$$\nu_s(z, \theta) = \frac{\delta(z, \theta)}{[1 + z_{rs}]} \nu'_s. \quad (6)$$

Finally, we get the total flux density through the integration of  $\nu_s(z, \theta)$  by  $z$ .

Calculating the differential SSC emission between  $z$  and  $z + dz$ , we need to compute soft photon density produced at layers with different Lorentz factors, which is given by  $u'_{ph} \simeq u'_{ph} \Gamma_{rela}^2$  (Dermer 1995; Georganopoulos & Kazanas 2003a).  $\Gamma_{rela}$  is the relative Lorentz factor between soft photons and IC electrons.  $u'_{ph}$  is soft photon energy density in the local frame. The photon energy density  $u(\nu'_s, z, \theta)$  is given by a sum of a local contribution (Kataoka et al. 1999):

$$u'_{loc}(\nu'_s, z) = \frac{3}{4} \frac{4\pi j'_s(\nu'_s, z)}{c \alpha'_s(\nu'_s, z)} [1 - \exp(-\alpha'_s(\nu'_s, z) R_0)], \quad (7)$$

and an external contribution:

$$u'_{ext}(\nu'_s, z, \theta) = \frac{j'_s(\nu'_s, z) \pi R_0^2}{c} \left[ \int_{z_0}^{z-R_0} \Gamma_{rela}^2(z_s, z, \theta) \frac{\exp[-\alpha'_s(\nu'_s, z)(z - z_s)] dz_s}{(z - z_s)^2} + \int_{z+R_0}^{z_{max}} \Gamma_{rela}^2(z_s, z, \theta) \frac{\exp[-\alpha'_s(\nu'_s, z)(z_s - z)] dz_s}{(z_s - z)^2} \right]. \quad (8)$$

Then the emission coefficient is given by (Inoue & Takahara 1996; Kataoka et al. 1999; Katarzynski et al. 2001)

$$j'_c(\nu'_c, z, \theta) = \frac{h}{4\pi} \epsilon'_c q(\epsilon'_c, z, \theta), \quad (9)$$

where  $q(\epsilon'_c, z, \theta)$  is the production rate of the differential photon:

$$q(\epsilon'_c, z, \theta) = \int d\epsilon'_s n_{ph}(\epsilon'_s, z, \theta) \int d\gamma N(\gamma, z) C(\epsilon'_c, \gamma, \epsilon'_s). \quad (10)$$

$C(\epsilon'_c, \gamma, \epsilon'_s)$  is the Compton kernel given by Jones (1968)

$$C(\epsilon'_c, \gamma, \epsilon'_s) = \frac{2\pi r_e^2 c}{\gamma^2 \epsilon'_s} [2\kappa \ln(\kappa) + (1 + 2\kappa)(1 - \kappa) + \frac{(4\epsilon'_s \gamma \kappa)^2}{2(1 + 4\epsilon'_s \gamma \kappa)} (1 - \kappa)], \quad (11)$$

where

$$\kappa = \frac{\epsilon'_c}{4\epsilon'_s\gamma(\gamma - \epsilon'_c)}, \quad (12)$$

and  $r_e$  is the classical electron radius. The integration of (10) follows the condition as:

$$\epsilon'_s \leq \epsilon'_c \leq \gamma \frac{4\epsilon'_s\gamma}{1 + 4\epsilon'_s\gamma}. \quad (13)$$

Then, we can integrate  $dL'_c(\nu'_c, z, \theta)$  to obtain the total flux density.

In calculating the differential EC emission between  $z$  and  $z + dz$ , we need to know soft photon energy density produced by external radiation field, we mainly consider the photons reprocessed by Broad Line Region (BLR)(Sikora et al. 1994). The photons are assumed to be distributed as a blackbody with temperature  $T_{ext}$ . In the comoving frame of each layer the mean soft photon energy is blueshifted to  $\epsilon'_{ext} \sim \Gamma(z)\epsilon_{ext} \sim \Gamma(z)k_B T_{ext}$ , where the  $k_B$  is the Boltzmann constant. The photon energy density is given by  $u'_{ph,ext} \sim u_{ph,ext}\Gamma^2(z)$ .

### 3.2. Radiation Model of Transverse Velocity Structures

To the transverse velocity structures, we replace the equation (3) by

$$dL'_s(\nu'_s, R, \theta) = 8\pi^2 R j'_s(\nu'_s)(z_{max} - z_0) e^{-\frac{\alpha'_s(\nu'_s)R_0}{s\Gamma\theta}} dR. \quad (14)$$

Soft photon energy density is given by:

$$u'(\nu'_s, R, \theta) = 2 \frac{2\pi j'_s(\nu'_s)}{c} \int_0^{\frac{z_{max}-z_0}{2}} dz \int_0^{R_0} dR_s \Gamma_{rel}^2(R_s, R, \theta) \frac{R_s \exp[-\alpha'_s(\nu'_s)(R^2 + z^2)^{1/2}]}{(R^2 + z^2)} \quad (15)$$

where  $R_s$  is the radius of producing the soft photons. Since the studied length is assumed to be short compared to the whole jet, we take the soft photon density at  $\frac{z_{max}-z_0}{2}$  in different  $z$  as an approximation. We find that this simplicity is reasonable in the following calculation.

## 4. Velocity Structure Constrained by Jet Power

In this section, we apply the transverse velocity structures constrained by jet power to the SEDs of Mrk 421 and 0716+714, and discuss their properties in the unification of BL Lac objects and FR I radio galaxies.

We select the well observed Mrk 421 that is a typically high energy peaked BL Lac (HBL). The SED of Mrk 421 is obtained by fitting the observed core data (for the quiescent state of Mrk 421, the data is from the Macomb et al. (1996) and NED) with our model. The SEDs of its parent population are then given by increasing the viewing angles. In this work, we adopt two kinds of transverse velocity structures  $\zeta = 0$  (uniform velocity structures) and  $\zeta = 1$  (bulk Lorentz factor linearly lessen from the center to the margin). The observed data of Mrk 421 are fitted using the parameters listed in Table 1. Its corresponding SEDs in different viewing angles are calculated to show the implications of velocity structures. Konopelko

et al. (2003) have used the one-zone SSC model to fit the lower state SEDs of Mrk 421 and obtained the parameters of  $s = 1.75$ ,  $\gamma_{max} = 3 \times 10^5$ ,  $B = 0.10G$ ; Blazejowski et al. (2005) have presented the parameters of  $\delta = 10$ ,  $B = 0.405G$ ,  $R = 0.7 \times 10^{16}cm$ . The parameters in our model are comparable to their ones. We set  $\Gamma_c = \Gamma_m = 10$  for the jet with uniform structure and  $\Gamma_m = 3$  for the jet with velocity structure (Ghisellini et al. (2005); Giroletti et al. (2004a); Tavecchio & Ghisellini (2008)). Assuming the same jet power for two structures, we can obtain  $\Gamma_c$  for the jet with velocity structure. The SEDs of Mrk 421 are shown in Fig. 1. The SEDs of two velocity structures show very small difference in the small viewing angle ( $3^\circ$ ). Under the viewing angle of parent population (FR I) ( $60^\circ$ ), the SEDs have large difference, in which the flux with velocity structure is much larger than ones with uniform structure. The velocity structure can resolve the problem that the observed FR I nuclei are over-luminous by a factor of  $10 - 10^4$  than ones predicted by simple one-zone model in optical and radio bands. In order to compare the observed and predicted fluxes of parent population, we also present two vertical lines denoting the optical (V band) and 5 GHz radio band respectively in Fig.1. It is noted that the radio fluxes given by the model are extrapolated from the infrared fluxes.

0716+714 is a typical low energy peaked BL Lac (LBL). We also list the parameters in the Table 1. Giommi et al. (1999) gave the magnetic field to be  $B > 0.9G$ . Tagliaferri et al. (2003) got the parameters of  $B = 2.5G$ ,  $R = 2 \times 10^{16}$ ,  $\theta = 3.4^\circ$ . These parameters are consistent with ones given by our model. The SEDs of 0716+714 given by the model are shown in Fig. 2. It is shown that the SEDs have obvious difference for two velocity structures under large viewing angles ( $40^\circ$  or  $60^\circ$ ).

In the Fig. 3, we give the luminosity ratio between the jets with  $\zeta = 1$  and  $\zeta = 0$  in three bands: radio (9GHz), optical (V band), and X-rays (1keV) for Mrk 421, 0716+714, and their parent population. It is shown that the ratio can reach 2 – 9 in three bands under large viewing angles corresponding to parent population. Understanding these properties, we present the variations of Doppler factors along the jet radius R for different velocity structures under the viewing angles of  $3^\circ$  and  $60^\circ$ , shown in Fig. 4 and 5. Under  $3^\circ$  (see the Fig. 4), the Doppler factor of the jet with velocity structure rapidly decreases with R and is smaller than ones of the jet with uniform velocity structure when  $R > 0.6R_0$ . However, the increase of the Doppler factor with R appears under  $60^\circ$  (Fig. 5).

In the unification scheme, it is believed that the appearance of AGNs strongly depends on the viewing angles and obscuration instead of intrinsic physical properties. For low luminosity radio-loud objects, such as BL Lac objects and FR I radio galaxies, the relativistic beaming effects caused by viewing angles should play an important role in observation. However, Chiaberge et al. (2000) have found that the observed FR I nuclei are over-luminous by a factor of  $10 - 10^4$  than ones predicted by simple one-zone model in the radio and optical bands. They have argued that a radial velocity structure, which a fast spine sur-

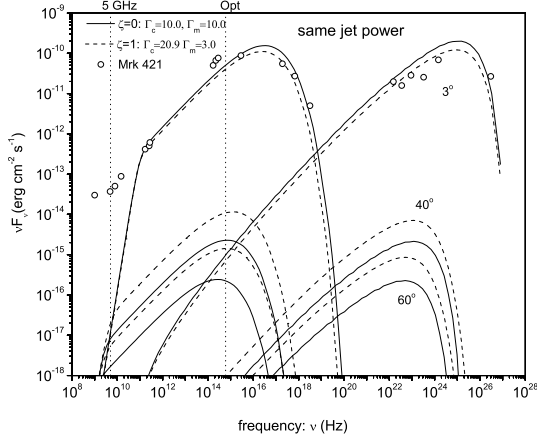


**Fig. 1.** The approximately fitting for data of Mrk 421 (from Macomb et al. (1996) and NED) and the extrapolated SEDs of parent population. The solid lines represent the emission of jet with uniform velocity structures ( $\zeta = 0$ ) and the dash lines denote the jet with velocity structures ( $\zeta = 1$ ). The upper two curves report the emission at angles of  $3^\circ$ , the mid and lower two curves are the cases of parent population of BL Lacs extrapolating the viewing angles to  $40^\circ$  and  $60^\circ$ .

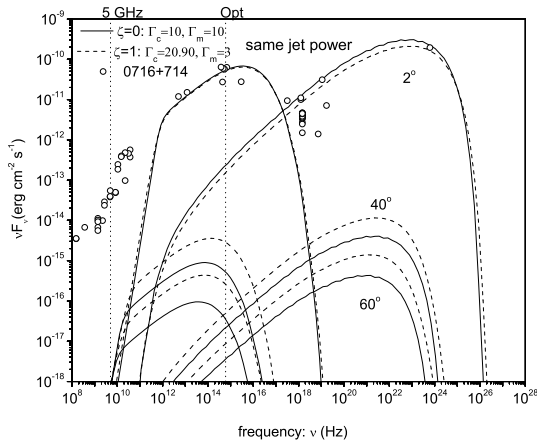


**Fig. 2.** The approximately fitting for NED data of 0716+714 and the extrapolated SEDs of parent population. The solid lines represent the jet with uniform velocity structures ( $\zeta = 0$ ) and the dash lines denote the jet with velocity structures ( $\zeta = 1$ ). The upper two curves report the emission at angles of  $2^\circ$ , the mid and lower two curves are the cases of parent population of BL Lacs extrapolating the viewing angles to  $40^\circ$  and  $60^\circ$ .

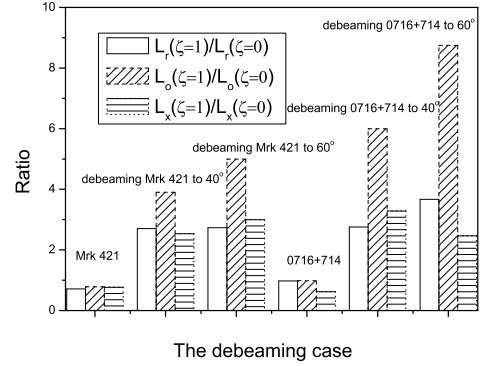


**Fig. 3.** The ratio of luminosity between  $\zeta = 1$  and  $\zeta = 0$  under different band and viewing angles.

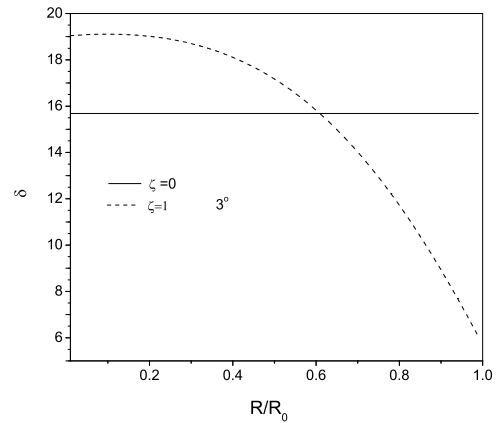


**Fig. 4.** Under  $\theta = 3^\circ$ , the Doppler factors vary with  $R$  for different velocity structures. Solid line denotes the case of uniform velocity structures and the dash line is in velocity structures.

rounded by a slow layer, can reconcile the above contradiction. We apply the velocity structures described previously to the unification of BLO and FRI. In Fig. 6, we show the debeaming trails with different velocity structures in the radio-optical luminosity plane for Mrk 421 and 0716+714. For Mrk 421, when the viewing angle is increased to  $60^\circ$ , the predicted optical and radio luminosity nearly come into the region of FRI in case of velocity structure, however they are less-luminous in case of uniform structure. For 0716+714, the predicted luminosity fully fall into the region of FRI in different velocity structures.

The  $\alpha_{ro}-\alpha_{ox}$  planes for Mrk 421, 0716+714 and FRI are presented in the Fig. 7, in which the lines denote the debeaming trails of Mrk 421 and 0716+714. The plotted data of FRI and BLO are from the Fossati et al. (1998) and Trussoni et al. (2003). For 0716+714, the debeamed indices fall into the region of FRI under different velocity structures. However, the debeamed indices of Mrk421

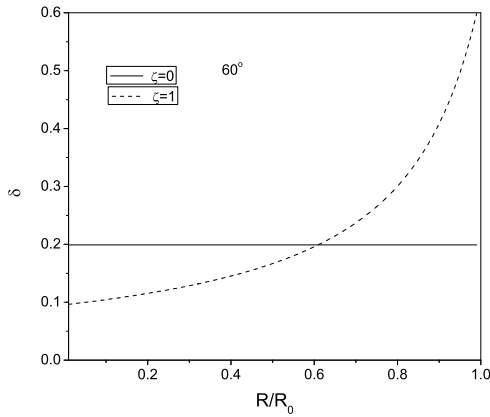


**Fig. 5.** Under  $\theta = 60^\circ$ , the Doppler factors vary with  $R$  for different velocity structures. Solid line denotes the case of uniform velocity structures and the dash line shows the case of velocity structures.

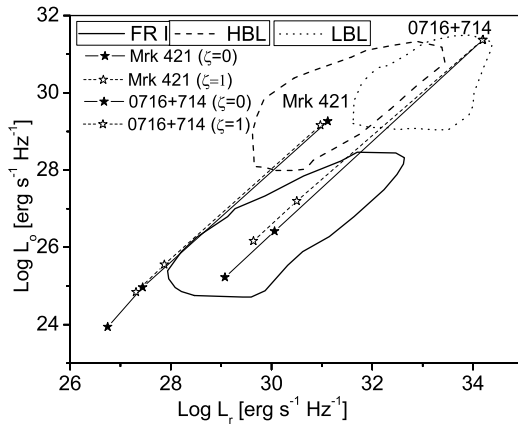


**Fig. 6.** Debeaming trails with the models of continual velocity structures in the radio-optical luminosity plane for Mrk 421 and 0716+714 (the solid lines denote  $\zeta = 0$  and dash ones are  $\zeta = 1$ ), where upper pentagrams correspond to the luminosity of BL Lacs at  $\theta = 2^\circ$  or  $3^\circ$  and lower ones are the predicted luminosity of parent population at  $\theta = 40^\circ$  and  $60^\circ$ . The three regions enclosed by curves respectively describe the range for three samples, i.e., HBL (dash curves), LBL (dot curves), and FR I (solid curves) in realistic observations (Chiaberge et al. 2000).

are marginally in the region of FRI. This implies some intrinsic physical difference exist between HBL and LBL.

## 5. Velocity Structure Constrained by Apparent Speed

In this section, we use the observed apparent speed to constrain the jet velocity structures and discuss its effect on the SEDs of BL Lac objects shown in Mrk 421 and 0716+714.

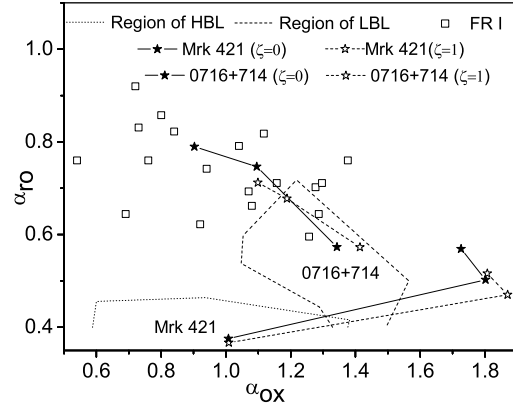


**Fig. 7.** Debeaming trails in the  $\alpha_{ox} - \alpha_{ro}$  plane for Mrk 421 and 0716+714. The solid denote  $\zeta = 0$  and dash lines is  $\zeta = 1$ . The lower pentagrams represent BL Lac, while the upper ones describe the parent population of BL Lac observed at  $\theta = 40^\circ$  and  $60^\circ$ . The data of FR I, HBL, and LBL are given by Fossati et al. (1998); Trussoni et al. (2003).

We take  $\beta_{app} = 3.6c$  to limit longitudinal and transverse velocity structures and calculate the SEDs of the jet with velocity structures to fit the observed data of Mrk 421 and 0716+714. Under  $\beta_{app} = 3.6c$ , adopting  $3^\circ$  or  $2^\circ$  as the viewing angles we obtain  $\Gamma_0$  for three kinds of longitudinal velocity structures, e.g. uniform ( $\xi = 0$ ), decelerating ( $\xi = -1$ ), and accelerating ( $\xi = 1$ ), which are listed in the figures. The SEDs of Mrk 421, 0716+714 and their parent populations under different velocity structures are shown in Fig. 8, 9, 10, and 11. It is shown that the elementary volume expansion ( $\xi > 0$ ) or compression ( $\xi < 0$ ) change the electron energy distribution in longitudinal bulk velocity structures and cause the parameters fitting the observed data to be large difference between uniform and velocity structure models (see the Table 1). In the decelerating velocity structures, we use smaller parameters of  $N_0$ ,  $\gamma_{max}$  and  $B$  to fit the observed SEDs compared to the uniform structure. On the contrary, we must use larger parameters in the accelerating models to fit the SEDs. When the velocity structures exist, the flux  $\nu F_\nu$  decreases slowly along the increase of the viewing angles (such as  $40^\circ$  or  $60^\circ$ ). However, the flux  $\nu F_\nu$  decreases quickly in the uniform structure. In the Fig. 12 and 13, we give the luminosity ratio between different viewing angles in the same band. In the uniform jet, the ratio changes greatly with the viewing angles. The energy equipartition between electron and magnetic field could not be true (Hardcastle et al. 1998). We find that for the acceleration velocity structures  $U_e/U_B$  has larger value (about 300) at the outside of studied jet scale, however, for the deceleration velocity structures the  $U_e$  is larger than  $U_B$  at the inner of studied jet scale, along the jet,  $U_B$  is became dominant at the outer (see the Fig. 14).

To the transverse velocity structures (Fig. 15 and 16), we adopt two kinds of velocity structures, e.g.  $\zeta = 0$  (uniform velocity structure) and  $\zeta = 1$  (bulk Lorentz factor

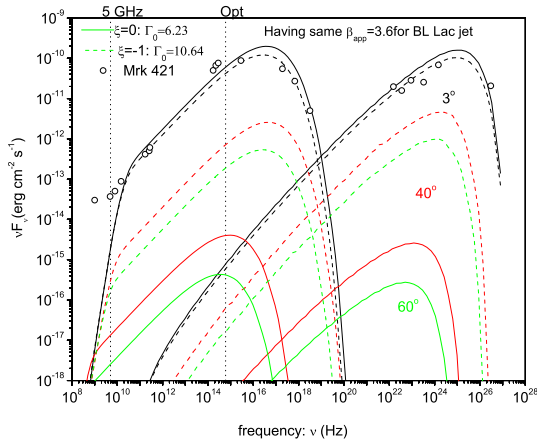


**Fig. 8.** Under  $\beta_{app} = 3.6c$ , the approximately fitting for data of Mrk 421 (from Macomb et al. (1996) and NED) and the extrapolated SEDs of parent population (Note that we use different parameters for different velocity structures, see the Table 1.). The solid lines represent the emission of jet with uniform velocity structures ( $\xi = 0$ ) and the dash lines denote the jet with velocity structures ( $\xi = -1$ ). The upper curves show the emission at angles of  $3^\circ$ , the red and green curves present parent population of BL Lacs with the viewing angles of  $40^\circ$  and  $60^\circ$ .

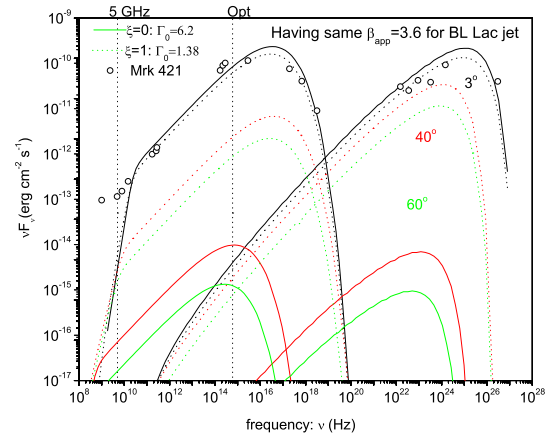


**Fig. 9.** Under  $\beta_{app} = 3.6c$ , the approximately fitting for data of Mrk 421 (from Macomb et al. (1996) and NED) (Note that we use different parameters for different velocity structures, see the Table 1.) and the extrapolated SEDs of parent population. The solid lines represent the emission of jet with uniform velocity structures ( $\xi = 0$ ) and the dot lines denote the jet with velocity structures ( $\xi = 1$ ). The upper curves report the emission at angles of  $3^\circ$ , the red and green curves present parent population of BL Lacs with the viewing angles of  $40^\circ$  and  $60^\circ$ .

linearly decreases from the center to the margin). We set  $\Gamma_m = 3$  and obtain  $\Gamma_c$  restricted by  $\beta_{app} = 3.6$ , which is listed in corresponding figures. The SEDs of Mrk 421 and 0716+714 in different viewing angles are shown in Fig. 15 and 16. We show that the lower luminosity is common to the jets with uniform velocity structure in large viewing angles, and that the way of solving the paradox of BLO and FRI unification is to consider the velocity structure, where all photons are not produced in same Doppler factor.

## 6. EC Spectra with Velocity Structure

Piner et al. (2007) have proposed that the mean fastest apparent speed for the quasars is  $6.8 \pm 1.1c$ , as the previous discussion we will use this observed apparent speed to constrain the parameters of velocity structures (i.e.,  $\Gamma_0 = 19.6$  for the  $\xi = -0.5$ ;  $\Gamma_0 = 8.4$  for the  $\xi = 0$ ). In the Fig. 17, under  $\beta_{app} = 6.8c$ , we present the fit for the data of FSRQ 3c 279 (Inoue & Takahara 1996). In the model, we set  $T_{ext} = 10eV$  (near the energy of hydrogen Lyman- $\alpha$  photons) and  $U_{ext} = 6.6 \times 10^{-5} \text{ erg cm}^{-3}$  for external photons, other parameters are shown in the Table 1. The solid lines represent the jet with uniform velocity structures ( $\xi = 0$ ) and the dot lines denote the jet with velocity structures ( $\xi = -0.5$ ). The upper curves show the emission with the angle of  $3^\circ$ , the mid and lower curves correspond to the parent population of quasars with the viewing angles of  $40^\circ$  and  $60^\circ$ . From the figure, firstly, we find that the observed EC component is weakly affected by velocity structures compared to synchrotron or SSC ones. The reason is that for continual jet the luminosity  $L_{EC}$  has the

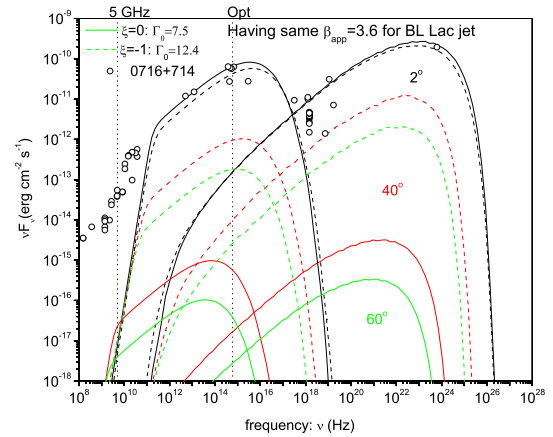


**Fig. 10.** Under  $\beta_{app} = 3.6c$ , the approximately fitting for NED data of 0716+714 (Note that we use different parameters for different velocity structures, see the Table 1.) and the extrapolated SEDs of parent population. The solid lines represent the jet with uniform velocity structures ( $\xi = 0$ ) and the dash lines denote the jet with velocity structures ( $\xi = -1$ ). The upper curves report the emission at angles of  $2^\circ$ , the red and green curves present parent population of BL Lacs with the viewing angles of  $40^\circ$  and  $60^\circ$ .

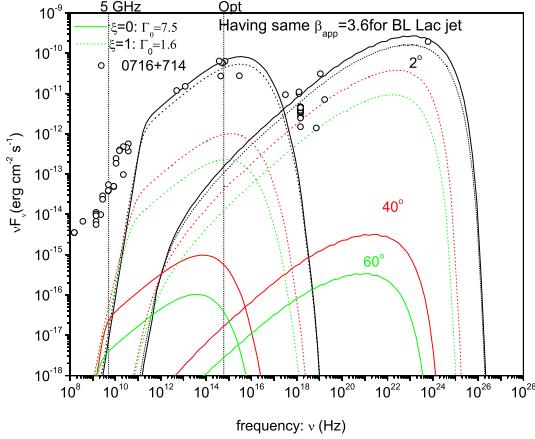


**Fig. 11.** Under  $\beta_{app} = 3.6c$ , the approximately fitting for NED data of 0716+714 (Note that we use different parameters for different velocity structures, see the Table 1.) and the extrapolated SEDs of parent population. The solid lines represent the jet with uniform velocity structures ( $\xi = 0$ ) and the dot lines denote the jet with velocity structures ( $\xi = 1$ ). The upper curves report the emission at angles of  $2^\circ$ , the red and green curves are present parent population of BL Lacs with the viewing angles of  $40^\circ$  and  $60^\circ$ .

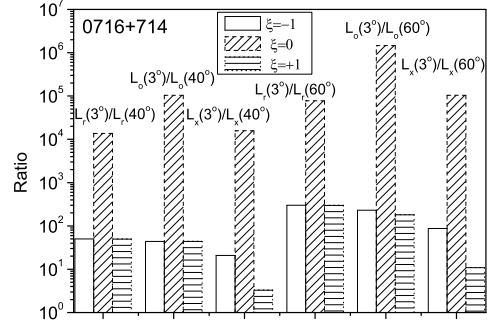


**Fig. 13.** The ratio of luminosity between different viewing angles under different  $\xi$  and bands for 0716+714.

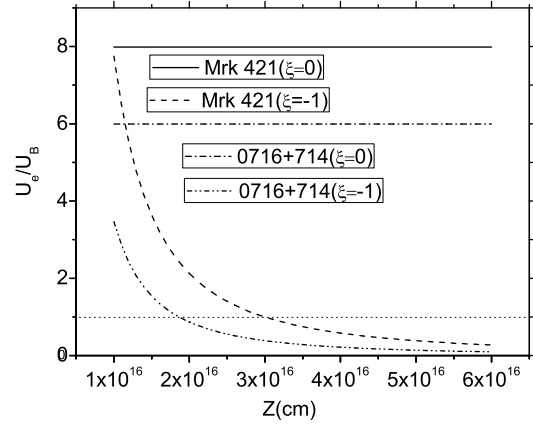


**Fig. 14.** The change of  $U_e/U_B$  with  $z$  in uniform and deceleration velocity structures. The dot line is  $U_e = U_B$ , solid ( $\xi = 0$ ) and dash lines ( $\xi = -1$ ) show Mrk 421, and the dash-dot ( $\xi = 0$ ) and dash-dot-dot lines ( $\xi = -1$ ) denote the 0716+714.

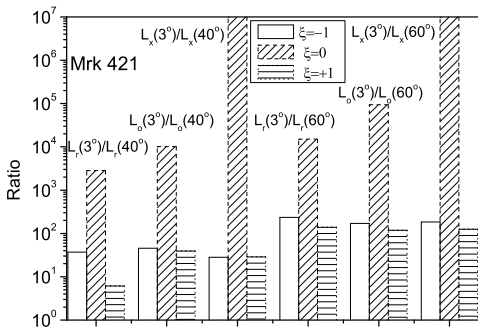


**Fig. 12.** The ratio of luminosity between different viewing angles under different  $\xi$  and bands for Mrk 421.

relation of  $L_{EC} \sim N_e \delta^3 \gamma'_{EC} \sim N_e \delta^3 U'_{ext} \sim \Gamma^2 \delta^3 U_{ext} N_e$ , the integration of  $\Gamma^2 \delta^3$  over  $z$  gives less discrepancy between the models of  $\xi = -0.5$  and  $\xi = 0$ .

## 7. Discussions and Conclusions

In this work we mainly pay attention to the influence of the bulk velocity structures on radiative spectra and ignore the radiative energy loss of the electrons in the studied jet scale. It is reasonable if we suppose ongoing particles acceleration in situ can compensate the radiative loss. However, radiative losses become important for high energy electrons producing the high energy part of synchrotron and IC emission, when the particles acceleration mechanism do not offset the radiative loss. In this situation, the high energy part of synchrotron and IC emission will be mainly originated at the base of jet, and their spectra will be steeper with the distance.

In this work, the synchrotron self-Compton (SSC) mod-

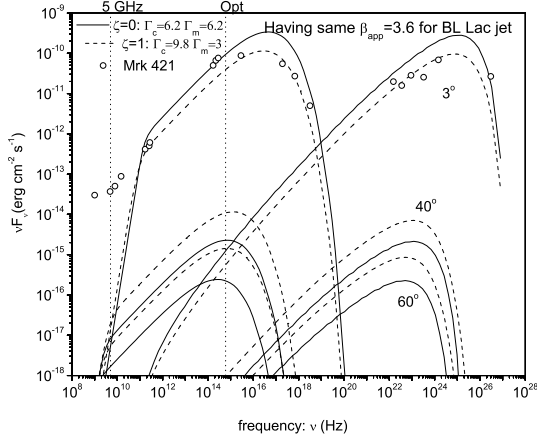


**Fig. 15.** Under  $\beta_{app} = 3.6c$ , the approximately fitting for data of Mrk 421 (from Macomb et al. (1996) and NED) and the extrapolated SEDs of parent population. The solid lines represent the emission of jet with uniform velocity structures ( $\zeta = 0$ ) and the dot lines denote the jet with velocity structures ( $\zeta = 1$ ). The upper curves show the emission at angles of  $3^\circ$ , the mid and lower curves present parent population of BL Lacs with the viewing angles of  $40^\circ$  and  $60^\circ$ .

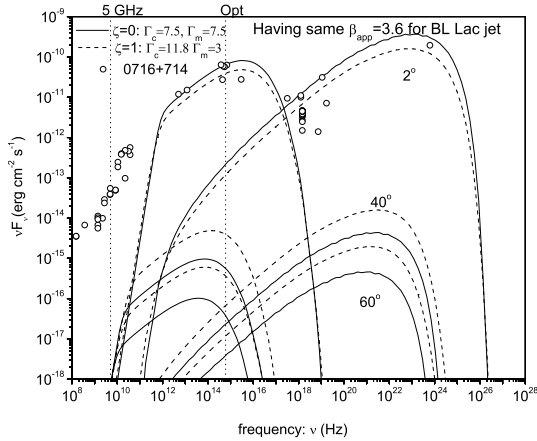


**Fig. 16.** Under  $\beta_{app} = 3.6c$ , the approximately fitting for NED data of 0716+714 and the extrapolated SEDs of parent population. The solid lines represent the jet with uniform velocity structures ( $\zeta = 0$ ) and the dash lines denote the jet with velocity structures ( $\zeta = 1$ ). The upper curves show the emission at angles of  $2^\circ$ , the mid and lower curves present parent population of BL Lacs with the viewing angles of  $40^\circ$  and  $60^\circ$ .

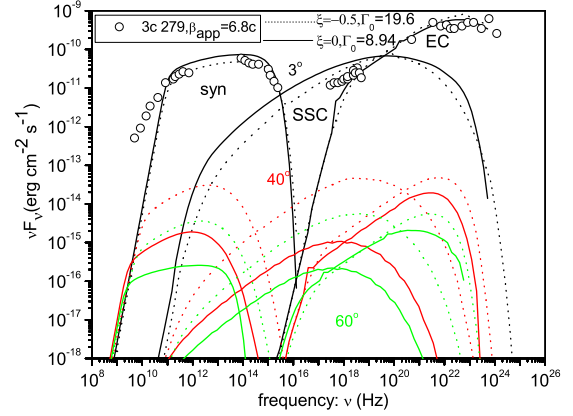


**Fig. 17.** Under  $\beta_{app} = 6.8c$ , the fit curve for data of FSRQ 3c 279 from the Inoue & Takahara (1996) with the models of uniform ( $\xi = 0$ ) or velocity structures ( $\xi = -0.5$ ) (Note that we use different parameters for different velocity structures, see the Table 1.) and the extrapolated SED of parent population. The solid lines represent the jet with uniform velocity structures ( $\xi = 0$ ) and the dot lines denote the jet with velocity structures ( $\xi = -0.5$ ). The upper curves show the emission at the angle of  $3^\circ$ , the red and green curves corresponds to the parent population of quasar with the viewing angles of  $40^\circ$  and  $60^\circ$ .

els and External Compton (EC) models of AGN jets with continually longitudinal and transverse bulk velocity structures are constructed. But our models can not discriminate a lateral and longitudinal deceleration scenario. For the former scenario we might observe the limb brightening in VLBI (Giroletti et al. 2004a). For the longitudinal deceleration scenario it should exist an outward-increasing radio-to-X-ray ratio (Georganopoulos & Kazanas 2003b). But they might be interrelated, for example, in a faster spine and slower layer model when the IC power is compared with the total bulk kinetic power. The Compton rocked effect will cause the spine to recoil and decelerate, and form the longitudinal velocity structures (Ghisellini et al. 2005). Similarly, if the gradual entrainment from external medium cause the jet deceleration, it would produce velocity gradients across the jet. A faster spine and a slower sheath are formed.

The rapid TeV flares observed for PKS 2155-304 and Mrk 501 (Aharonian et al. 2007; Albert et al. 2007) appears to indicate large bulk Lorentz factors. The systematic differences of the Doppler factors inferred from different waveband observations indicate that the jet holds velocity structures within sub-parsec to parsec scale. Based on our calculation, large bulk Lorentz factor in the base of jet for longitudinal velocity structures or in the spine for transverse velocity structures, can satisfy the TeV photon escape, where the apparent speed is moderate.

In the unified schemes, we find that beside the viewing angles, the bulk velocity structures play an important role in the Doppler beaming pattern. Firstly, from the observed data to deduce the intrinsic quantities, the velocity structures and the viewing angles should be considered at

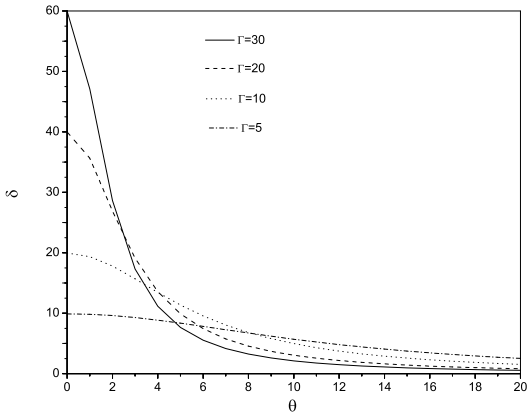


**Fig. 18.** For different bulk Lorentz factor of 30, 20, 10 and 5, the Doppler factors vary with the view angles.

one time. In fact, if the jets have velocity structures, their intrinsic flux will be difficultly deduced under different viewing angles. Secondly, the velocity structures also bring some statistical discrepancy between observation and theory in simple one-zone model (Chiaberge et al. 2000; Henri & Sauge 2006). In one-zone model, if  $\theta \leq 1/\Gamma$ , one has  $1 \leq \delta \leq 2\Gamma$  except  $\delta \approx 1/\Gamma$ . This means that for a few Doppler amplified sources, one expects a large number of unbeamed counterparts. In this work, we find that under larger viewing angles the velocity structures limited by apparent speed have larger effect on the observed flux. The statistic of the flux limited sources will provide a framework to explore the velocity structures of AGN jets.

In the Fig. 18 also given by Urry & Padovani (1995), we present the relations between Doppler factor, Lorentz factor and viewing angle. The curve lines for different Lorentz factors cross each other within the viewing angles of  $1^\circ$  to  $10^\circ$ . They show that large bulk Lorentz factor does not always produce large Doppler factor when the viewing angle increases. Furthermore, the Doppler factor with large Lorentz factor decreases quickly under the increase of viewing angles. These properties cause complex effects on emissive spectra.

The observed apparent speed might be the results of flux convolution over the resolution region, which can solve the inconsistency of bulk motions obtained by different wavebands. We find that the influences of the velocity structures upon the observed spectra heavily depend on the viewing angles. Under the jet with velocity structure constrained by jet power and apparent speed, we show that the SEDs have large difference for the jets with and without velocity structure in large viewing angle. For the jet with transverse and longitudinal deceleration velocity structure, its flux is much larger than one with uniform structure. Especially, in longitudinal bulk velocity structures, as the elementary volume expansion ( $\xi > 0$ ) or compression ( $\xi < 0$ ) greatly change the electron energy distri-

bution, we use smaller values of  $N_0$ ,  $\gamma_{max}$  and  $B$  than the uniform ones to fit the SEDs; on the contrary, we must use larger values for the accelerating models to get fitting. We find that for the deceleration velocity structures the  $U_e$  is larger than  $U_B$  at the inner of studied jet scale, along the jet,  $U_B$  is became dominant at the outer. The EC observed spectra are weakly affected by velocity structures compared to synchrotron and SSC ones.

Nowadays, the VLBA can not resolve the velocity structures with sub-parsec to parsec scale, the AGN's unified schemes exit a large uncertainty. The TeV emission is easily produced in the jet with large velocity structures and indicates that TeV blazars should have the jet bulk velocity structures within sub-parsec to parsec scale.

We thank the anonymous referee for useful comments that led to improvements in the paper. We acknowledge the financial supports from the National Natural Science Foundation of China 10673028, 10778702 and 10803018, and the National Basic Research Program of China (973 Program 2009CB824800). This research made use of the NASA/IPAC Extragalactic Database (NED) which is operated by the Jet Propulsion Laboratory, California Institute of Technology, under contract with the National Aeronautics and Space Administration.

**Table 1.** Input parameters of the models for the Mrk 421, 0716+714 and 3c 279. The unit of the  $z_0$ ,  $z_{max}$ , and  $R$  are cm; B is Gauss

Objects	$n_0$	$\gamma_{max}$	Index	$z_0$	$z_{max}$	R	B	$\theta$
Mrk 421( $\zeta = 0, 1$ )	$3.9 \times 10^2$	$8.0 \times 10^4$	1.8	$1 \times 10^{16}$	$6 \times 10^{16}$	$1 \times 10^{16}$	0.18	$3^\circ$
Mrk 421( $\xi = 0$ )	$4.3 \times 10^2$	$8.0 \times 10^4$	1.8	$1 \times 10^{16}$	$6 \times 10^{16}$	$1 \times 10^{16}$	0.24	$3^\circ$
Mrk 421( $\xi = -1$ )	$1.0 \times 10^2$	$7.0 \times 10^4$	1.8	$1 \times 10^{16}$	$6 \times 10^{16}$	$1 \times 10^{16}$	0.1	$3^\circ$
Mrk 421( $\xi = 1$ )	$1.0 \times 10^4$	$1.0 \times 10^5$	1.8	$1 \times 10^{16}$	$6 \times 10^{16}$	$1 \times 10^{16}$	0.9	$3^\circ$
0716+714( $\zeta = 0, 1$ )	$4.6 \times 10^4$	$8.0 \times 10^3$	2.0	$1 \times 10^{16}$	$6 \times 10^{16}$	$1 \times 10^{16}$	1.0	$2^\circ$
0716+714( $\xi = 0$ )	$5.0 \times 10^4$	$8.0 \times 10^3$	2.0	$1 \times 10^{16}$	$6 \times 10^{16}$	$1 \times 10^{16}$	1.2	$2^\circ$
0716+714( $\xi = -1$ )	$1.0 \times 10^4$	$7.0 \times 10^3$	2.0	$1 \times 10^{16}$	$6 \times 10^{16}$	$1 \times 10^{16}$	0.7	$2^\circ$
0716+714( $\xi = 1$ )	$1.0 \times 10^6$	$1.0 \times 10^4$	2.0	$1 \times 10^{16}$	$6 \times 10^{16}$	$1 \times 10^{16}$	5.0	$2^\circ$
3c279( $\xi = 0$ )	$8.0 \times 10^3$	$1.0 \times 10^3$	2.0	$1 \times 10^{16}$	$2 \times 10^{17}$	$1 \times 10^{17}$	1.4	$3^\circ$
3c279( $\xi = -0.5$ )	$1.0 \times 10^3$	$9.0 \times 10^2$	2.0	$1 \times 10^{16}$	$2 \times 10^{17}$	$1 \times 10^{17}$	0.35	$3^\circ$

**References**

- Aharonian, F., et al. 2007, *ApJ* 664, L71  
 Albert, J., et al. 2007, *ApJ* 669, 882  
 Begelman, M. C., Fabian, A. C., & Rees, M. J. 2008, *MNRAS*, 384, L19  
 Blandford, R. D., & Levinson, A. 1995, *ApJ*, 441, 79  
 Blazewski, M., et al. 2005, *ApJ*, 630, 130  
 Celotti, A., Padovani, P., & Ghisellini, G. 1997, *MNRAS*, 286, 415  
 Chiaberge, M., Celotti, A., Capetti, A., & Ghisellini, G. 2000, *A&A*, 358, 104  
 Condon, J. J., et al. 1998, *AJ*, 115, 1693  
 Dermer, C. D., 1995, *ApJ*, 446, L63  
 Finke, J., Dermer, C., Bottcher, M. 2008, *ApJ*, 686, 181  
 Fossati, G., Maraschi, L., Celotti, A., Comastri, A., & Ghisellini, G. 1998, *MNRAS*, 299, 433  
 Georganopoulos, M., & Marscher, A. P. 1998, *ApJ*, 506, 621  
 Georganopoulos, M., & Kazanas, D. 2003a, *ApJ*, 594, L27  
 Georganopoulos, M., & Kazanas, D. 2003b, *ApJ*, 589, L5  
 Georganopoulos, M., & Kazanas, D. 2004, *ApJ*, 604, L81  
 Georganopoulos, M., Perlman, E. S., & Kazanas, D. 2005, *ApJ*, 634, L33  
 Ghisellini, G., Maraschi, L., & Treves, A. 1985, *A&A*, 146, 204  
 Ghisellini, G., Tavecchio, F., & Chiaberge, M. 2005, *A&A*, 432, 401  
 Ghisellini, G., & Tavecchio, F. 2008, *MNRAS*, 386, L28  
 Giommi, P., Massaro, E., Chiappetti, L., et al. 1999, *A&A*, 351, 59  
 Giroletti, M., Giovannini, G., Feretti, E., et al. 2004a, *ApJ*, 600, 127  
 Giroletti, M., Giovannini, G., Taylor, G. B., & Falomo, R. 2004b, *ApJ*, 613, 752  
 Gopal-Krishna, Dhurde S., Wiita P. J., 2004, *ApJ*, 615, L81  
 Gopal-Krishna, Wiita P. J., Dhurde S., 2006, *MNRAS*, 369, 1287  
 Gopal-Krishna, Dhurde S., Sircar. P., Wiita P. J., 2007, *MNRAS*, 377, 446  
 Hardcastle, M. J., Birkinshaw, M., & Worrall, D. M. 1998, *MNRAS*, 294, 615  
 Henri, G., & Sauge, L. 2006, *ApJ*, 640, 185  
 Inoue, S., & Takahara, F. 1996, *ApJ*, 463, 555  
 Jones, F. C. 1968, *Phys. Rev.*, 167, 1159  
 Kataoka, J., Mattox, J. R., Quinn, J., et al. 1999, *ApJ*, 514, 138  
 Katarzynski, K., Sol, H., & Kus. A. 2001, *A&A*, 367, 809  
 Konopelko A., Mastichiadis A., Kirk J., de Jager O. C., Stecker F.W. 2003, *ApJ*, 597, 851  
 Krawczynski, H., Coppi, P. S., & Aharonian, F. 2002, *MNRAS*, 336, 721  
 Li, H., & Wang, J. 2004, *ApJ*, 617, 162  
 Macomb, D. J., Akerlof, C. W., Aller, H. D., et al. 1996, *ApJ*, 459, L111  
 Marscher, A. P. 1980, *ApJ*, 235, 386  
 Piner, B. G. & Edwards, P. G. 2004, *ApJ*, 600, 115  
 Piner, B. G., Mahmud, M., Fey, A. L., Gospodinova, K. 2007, *AJ*, 133:2357  
 Piner, B. G., Pant, N., & Edwards, P. G. 2008, *ApJ*, 678, 64  
 Rybicki, G., & Lightman, A. P. 1979, *Radiative Processes in Astrophysics* (Wiley Interscience, New York)  
 Sikora, M., Begelman, M. C., & Rees, M. J. 1994, *ApJ*, 421, 153  
 Tagliaferri, G. 2003, *A&A*, 400, 477  
 Tavecchio, F., & Ghisellini, G. 2008, *MNRAS*, 385, L98  
 Trussoni, E., Capetti, A., Celotti, A., et al. 2003, *A&A*, 403, 889  
 Wang, J., Li, H., & Xue, L. 2004, *ApJ*, 617, 113  
 Urry, C. M., & Padovani, P. 1995, *PASP*, 107, 803  
 Vermeulen R. C., Cohen M. H., 1994, *ApJ*, 430, 467